Eur. J. Mech., B/Fluids, **17**, n° 1, 105-136, 1998

The effect of drag-reducing polymer additives on wall-pressure fluctuations in turbulent channel flows

L. JOURDAN *, Y. KNAPP *, F. OLIVER ** and J. P. GUIBERGIA **

ABSTRACT. – The present paper is concerned with the experimental study of the influence of Toms' phenomenon on the convective part of the hydrodynamic turbulent wall-pressure field. The experiments were carried out in a water tunnel, at flow velocities of 2.3, 3.3 and 4.3 m/s, where amounts of drag reduction up to 40% were obtained by injecting dilute polymer solutions. An investigation of the spectral feature of the wall-pressure frequency spectrum and the wall-pressure frequency cross-spectrum was achieved from data taken using pinhole transducers. The scaling laws for the mid- and high-frequency regions of the spectrum were examined both for the water flow and the drag-reducing flow. The use of a noise cancellation procedure allowed observation of the maximum of the spectrum in the mid-frequency range at an approximately reduced frequency $\omega\delta/u_\tau$ of 80 for the water flow. This maximum is shifted towards a higher value of the reduced frequency in the presence of Toms' effect. From cross-spectral data obtained over separation distances ranging from 0.4 δ to 2.8 δ, the effect of drag reduction was estimated on the coherence functions as well as the convection velocity. These data show a correlated shift of the threshold which delineates the low wave number group identified as the large-scale turbulence contributor in the outer region of the flow and the high wave number group associated with turbulent sources in the log-region. The effect of drag reduction on the convection velocity data supports the fact that the contributions to the different wave number groups should be attributable to activity in the outer and inner regions, respectively. In addition, a computation of the root mean square pressure was achieved from the wall-pressure frequency spectrum. When expressed as functions of the percentage of drag reduction, the rms pressures related to the wall shear stress are found to increase monotonicaly. The equivalent ratio obtained by scaling the rms pressures using the dynamic pressure is found to decrease in the drag-reducing flow. Finally, an estimation of the probability density distribution showed that the skin friction reduction affects predominantly the occurrence of higher pressure amplitudes as well as very low pressure amplitudes. This confirms the important contribution of the large pressure peak events to the overall features of the wall-pressure. © Elsevier, Paris.

1. Introduction

The investigation of the wall-pressure field beneath the turbulent boundary layer is of special interest with respect to flow noise generation and flow-induced structural vibrations. For the purpose of reducing undesirable effects associated with the turbulent environment, understanding of the main dynamical mechanisms leading to wall-pressure fluctuations is essential. The generation of wall-pressure fluctuations beneath a turbulent boundary layer is coupled to the dynamics of the instantaneous velocity field throughout the entire boundary layer. This coupling is expressed in terms of Poisson's equation

* FLUIDATA, Pépinière de l'IcEM, IMT Technopôle de Château Gombert, 13451 Marseille cedex 20, France.

** Ecole Supérieure de Mécanique de Marseille, IMT Technopôle de Château Gombert, 13451 Marseille cedex 20, France.

0997-7546/98/01/© Elsevier, Paris

through the interaction between the fluctuating velocity field and the mean shear as well as the non linear interaction of the velocity fluctuations with themselves. Moreover, since the instantaneous gradients of the pressure fluctuations are equal to the flux of vorticity from the wall, the wall-pressure fluctuations are intimately related to the vorticity fluctuations and the organisation of the turbulent structures within the boundary layer. In order to characterize the mechanisms which generate wall-pressure fluctuations, the questions to be answered are: What pressure contribution is relevant to each type of interaction? Does the first or the second term of Poisson's equation play the dominant role? In addition, the problem of establishing the location of the flow structures predominantly responsible for the generation of wall-pressure fluctuations arises.

From the formal solution for the fluctuating component of the wall-pressure field (which can be written as a Poisson integral) it can be established that the contributions to the high-frequency part of the spectrum should be attributed to turbulence activity located in the near wall-region, whereas the lower portion of the spectrum can originate from activities throughout the entire boundary layer. Further indications of the spatial location of the pressure sources in the multilayer turbulent boundary layer can be obtained by observing the collapse of the spectral data using the inner and outer flow scaling variables. In particular, a universal collapse of the low-, mid- and high-frequency regions of the spectra over a range of flow speeds is achieved in an equilibrium turbulent boundary layer. Finally, additional information concerning the correlation between detailed features of organised events and the wall-pressure signatures can be provided by using of conditional averaging techniques. Such techniques have been used to study the coupling between high amplitude pressure peaks and flow structures in the near wall region of the turbulent boundary layer. Notably, Johanson *et al.* (1981) made use of the VITA technique to observe a linear relationship between the amplitudes of the pressure peaks and the amplitude of the velocity patterns. The existence of such a relationship indicates that the turbulence/mean-shear interaction plays a dominant role in the generation of high amplitude wall-pressure peaks. Furthermore, the detection of strong inclined buffer shear layers (extending from the wall to the edge of the logarithmic region) accompanying the occurrence of large positive peaks, suggests that the wall-pressure sources could be interpreted in terms of individual hairpin vortices as observed in the near wall region of the boundary layer.

In order to control the mechanism responsible for the generation of wall-pressure fluctuations, the present work aimed at acting on the dynamics of the near wall region directly concerned with the occurrence of high amplitude pressure peaks. For this purpose, the balance between the turbulence production and the dissipation was perturbed by generating dractic amounts of drag reduction in the turbulent boundary layer. As a matter of fact, since the turbulence production is intimately connected to the dynamics of the buffer region, and the wall shear stress is proportional to the energy dissipation of the flow, the reduction of the wall shear stress affects the process responsible for the occurrence of large pressure peaks. Here, the drag reduction was achieved by injecting dilute solutions of high molecular weight polymers into a fully developed turbulent flow. This technique is of special interest in so far as very large amounts of drag reduction can be obtained.

An examination of the spectral features of the frequency spectra and frequency cross-spectra measured in the water flow and in the presence of drag reduction, is the main emphasis of the paper. Additional indications of the statistical properties of the wall-pressure field were obtained by estimating the rms pressures and the probability distributions of the pressure amplitudes. The data were measured using pinhole sensors and a noise cancellation procedure was utilised to attenuate the effect of facility-related noise contamination on the results. This procedure allowed observation of the influence of drag reduction on the location of the maximum of the spectrum. Moreover, the cross-spectral data allowed examination of the effect of Toms' phenomenon (Toms, 1948) on the decay as well as the convective behaviour of the surface pressure field.

2. Experimental procedure

2.1. Flow system

All experiments were carried out in the water tunnel at the Institut de Mécanique des Fluides de Marseille under conditions of hydraulically smooth flow surfaces. A description of the facility is given in Scheme A. The transparent test section has a length of 1 m and a rectangular cross-section of 0.25×0.03 m^2. These dimensions provide fully developed turbulent flows at the measurement location over the velocity range 1-5 m/s and ensure two-dimensional properties in the central region of the working section where sidewall effects are negligible. In order to minimize contamination of the pressure measurements by acoustic and vibratory contributions, the motor and pump are uncoupled from the duct by means of coupling sleeves and a insulating vessel is placed downstream from the pump to attenuate the propagation of radiated acoustic waves. For the purpose of generating Toms' effect, dilute solutions of high molecular weight ($M \approx 16 \times 10^6$) polyacrylamides were injected from a pressurised tank into the turbulent water flow. The injection system used provided injections of polymer over the whole cross-section of the flow by means of a comb injector. The injector was located 40 hydraulic diameters upstream from the entrance of the working section so as to obtain a constant polymer concentration in the test section area.

2.2. Flow conditions and measurement technique

The experiments were carried out in three reference water flows at respective centreline velocities of 2.3, 3.3 and 4.3 m/s. For these velocities, the flow in the measurement region was typical of fully developed, two-dimensional channel flow. This condition was guaranteed by measuring the mean velocity (*Fig.* 1(a)-1(b)) and turbulent intensity (*Fig.* 2) profiles over the half height of the test section at the different velocities. Here, the value of 2.3 m/s was the lower limit of the velocity range selected for the purpose of generating sufficiently high rates of drag reduction. The reference flow parameters were measured in terms of mean streamwise centreline velocity, bulk velocity, wall-pressure fluctuations and average wall shear stress. The influence of the additives on the flow

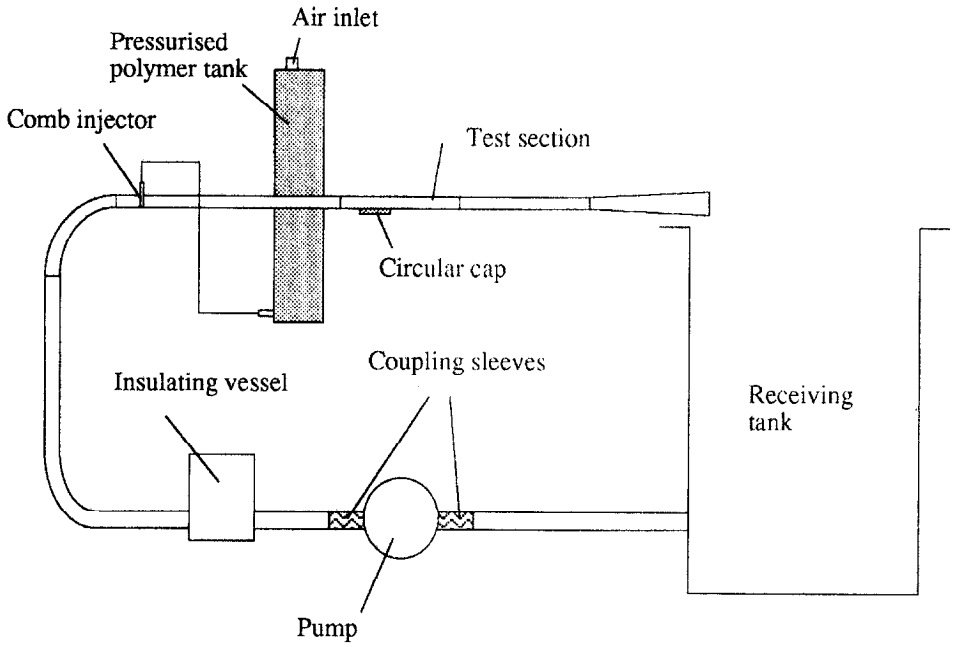

Scheme A. – Experimental Facility.

properties was estimated by taking simultaneous measurements of the latter parameters when the injection was performed.

To take into account the effect of the injection alone, the flow parameters were measured when water or dilute solutions were injected at similar rates. The concentration of the injected dilute polymer solutions was 2000 wppm and the injection was performed at rates ranging from 10 to 100 cm^3/s. The maximum value of the injection rate was limited to 100 cm^3/s in order to avoid a perturbation of the velocity field in the test section owing to the injection process. The ratio of the injection rate to the total flow rate did not exceed the value of 0.006 over the selected range. For the present flow conditions, Toms' phenomenon could be assumed to appear locally downstream from the injection zone with respect to the critical value of the concentration that must be reached for generating the onset of drag reduction.

The centreline velocity and the bulk velocity were estimated in the reference flows from the measurement of the mean stremwise velocity profile using the Laser Doppler Velocimetry technique. The light source used was a 1 W, 514.5 nm Spectra Physics Argon-Ion Laser and the optical components were arranged in the backward scatter mode. The 5.1° beam intersection angle and a beam diameter of 1.25 mm gave scattering volume dimensions of 3.7 mm length in the spanwise direction and 0.17 mm in diameter both at the $1/e^2$ intensity points. The estimation of the mean velocity profiles and the turbulent intensity distributions were derived using a Dantec Burst Spectrum Analyser. These measurements were performed 20 cm downstream from the entrance of the test section at the location of the wall-pressure fluctuation measurements.

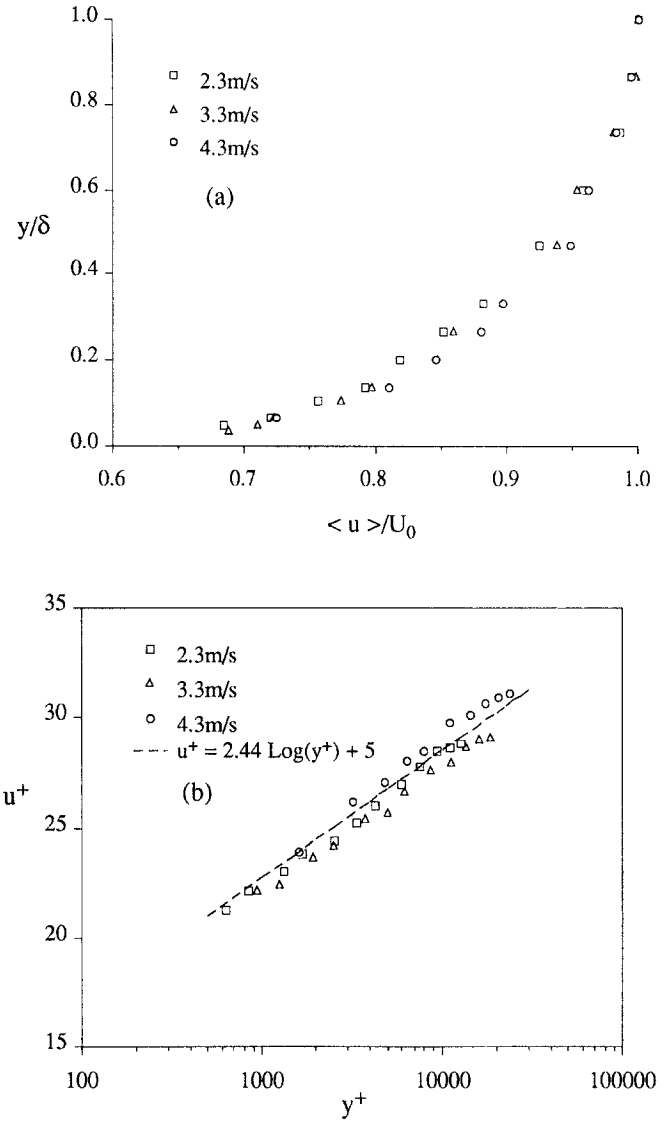

Fig. 1(a)-(b). – Mean streamwise velocity profiles measured in the water flows at different velocities: (a) outer variable scaling, (b) viscous scale normalization.

The measurements of the wall-pressure fluctuations were carried out using an array of four PCB A-116 piezoelectric transducers. Each transducer was mounted in a cavity in order to minimize the effect of spatial averaging at high frequency. This technique allows reduction of the size of the transducer sensitive area to the pinhole cavity dimension. Different sizes of cavity pinholes were tested (from 0.4 to 1 mm), and a convenient compromise was found to be 0.8 mm owing to the great loss of sensitivity observed for very small pinhole dimensions. The cavity volume was adjusted so as to ensure that the Helmotz resonance of the mounting was above the frequency range of interest in the wall-pressure measurements. The transducers were located along one diameter of a circular disc which was mounted flush on the lower side of the test section. The array

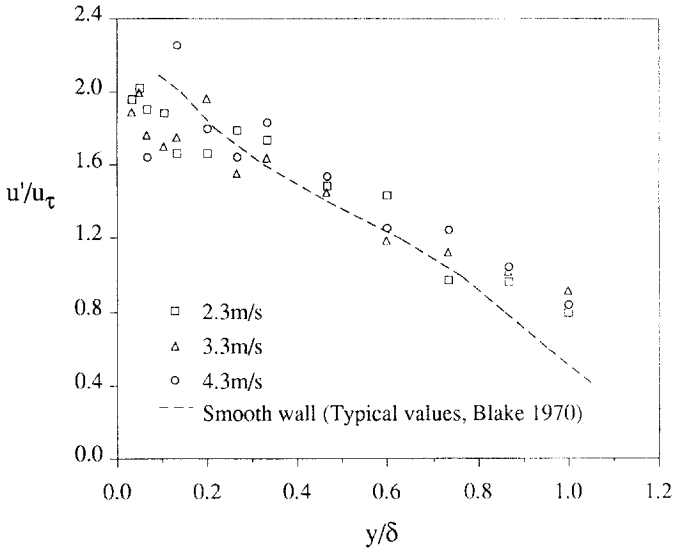

Fig. 2. – Streamwise turbulence intensities measured in the water flows at different velocities.

of transducers could be aligned either parallel or perpendicular to the flow direction with a view to measuring the cross-spectral statistics of the wall-pressure field. The set of separation distances between the consecutive pinhole locations could provide spacings ranging from 6 to 42 mm.

As argued by many authors, difficulty in measuring the wall-pressure fluctuations arises from low frequency contamination by facility-related noise and the limitation of the high frequency range owing to the spatial resolution of the pressure transducer. For the purpose of measuring the influence of drag reduction on the spectra at low frequency, the wall-pressure measurements were decontamined (below 50 Hz) using a noise cancellation technique based on the temporal difference of two spanwise transducer signals. This technique allowed efficient decontamination of the wall-pressure spectra measured at the velocity of 4.3 m/s.

To calibrate the array of transducers, the disc was placed at the end of a Kundt tube excited with a 0-5 kHz random noise. The tube was designed so as to ensure plane wave propagation over the frequency range 0-2.5 kHz. Note that this frequency domain is larger than the frequency range of the spectra measured at the maximum value of the flow velocity. The calibration consisted of estimating the transfer function between each pinhole sensor and a reference transducer which was mounted flush at the centre of the disc. A typical calibration curve of a cavity mounted transducer is illustrated in Figure 3 over the frequency range $\omega R_T/U_c \leq 1$ (where R_T is the radius of the pinhole, and U_c is the frequency dependent convection velocity of the pressure sources), estimated for the highest velocity used in our experiments. The wall-pressure data acquisitions were obtained with a four channel fast Fourier transform analyser within the frequency band 0-5 kHz. The signal analysis consisted of functions averaged over 256 frames of 4096 points.

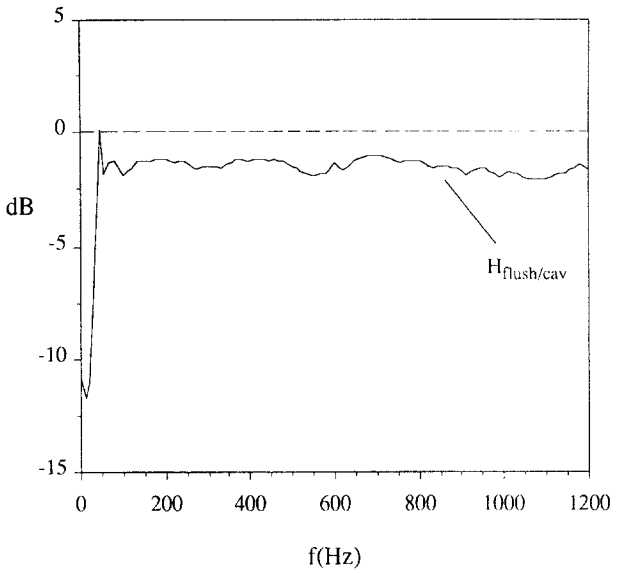

Fig. 3. – Typical magnitude curve of the transfer function measured between the reference flush mounted transducer and a cavity mounted transducer.

The mean value of the wall shear stress was measured in the vicinity of the pressure transducers by estimating the loss of static pressure over a 40 cm distance centred on the disc position. The pressure loss was evaluated using two 1 mm diameter pressure taps aligned with the centreline of the test section and connected to a differential pressure transducer Validyne DP15TL. The pressure drop was estimated within the range of ± 8618 Pa with an accuracy of ± 15 Pa. A calibration of the shear stress measurements was obtained by matching data from reference water flows to Konakov's law (Nekrassov, 1978) over the velocity range 1-5 m/s. The percentage of drag reduction was estimated as the ratio:

$$\text{DR}\% = 100.[(\Delta P_s - \Delta P_p)/\Delta P_s]_Q \tag{1}$$

where ΔP_s is the pressure drop measured between the taps in the pure water flow and ΔP_p is the pressure loss measured in the presence of the additives at comparable flow rate Q.

3. Results and discussion

3.1. Spectral features of wall-pressure fluctuations

In order to validate the measurements of the wall-pressure fluctuation spectra, the effect of sensor resolution was initially examined in the case of pure water flow. The frequency range over which the data are not affected by the averaging effect of the sensor is expected to extend to higher frequencies in the presence of drag reduction since

the transducer size as expressed in terms of viscous units diminishes with decreasing values of the shear velocity.

For the water reference flows, the dimensionless transducers sizes were $d^+ = 74$, 104, 136 at 2.3, 3.3 and 4.3 m/s, respectively. The corresponding Reynolds numbers, based on the shear velocity and the channel half-width δ, were 1400, 1950 and 2550. Such values for the Reynolds number are higher than the minimal value suggested by Panton and Linebarger (1974) for the contribution of the turbulence activity in the log-law region to become apparent in the spectra. Notably, this overlap region appears to occur in the frequency range $100 \leq \omega\delta/u_\tau \leq 0.3\,\mathrm{Re}_\tau$ ($\mathrm{Re}_\tau = u_\tau\delta/\nu$) in the turbulent boundary layer, as established by Farabee and Casarella (1991). Assuming uniform sensitivity distribution over the surface of the circular sensors, the spectral frequency range over which the sensor spatial resolution effects are not prejudicial was estimated from Corcos (1963) correction procedure. This correction method predicts that attenuation of the spectral level, due to the lack of sensor resolution, will occur above the critical threshold $\omega R_T/U_c \approx 1$. For the present flow conditions, the ratio U_c/U_0 (U_0 is the centreline velocity) reached an asymptotic value of 0.66 at high frequency, in the pure water flows, and the values of the cut off frequency obtained from equating the ratio $\omega R_T/0.06\,U_0$ to unity were estimated as 604, 866 and 1130 Hz, at 2.3, 3.3 and 4.4 m/s. Such values for the cut off frequencies correspond to an approximately constant value of the reduced frequency $\omega\delta/u_\tau \approx 620$ which is more than $0.3\,\mathrm{Re}_\tau$ at the flow velocities of 2.3 and 3.3 m/s, and lies within the frequency range $100 \leq \omega\delta/u_\tau \leq 0.3\,\mathrm{Re}_\tau$ at 4.3 m/s. Thus, the attenuating effect of the sensor is expected to occur in the high frequency range (above the overlap region) where the scaling behaviour of the spectra should follow a $\omega^{-7/3}$ decay rate, at 2.3 and 3.3 m/s. For the flow velocity of 4.3 m/s, this attenuating effect is expected to lie in the overlap region where the normalized spectra should exhibit a -1 slope.

In order to observe the effect of the additives in the low frequency range, a noise cancellation procedure was performed on the data. As previously mentioned, this technique did not allow efficient decontamination of the spectra at 2.3 and 3.3 m/s. The noise cancellation procedure used to filter the facility-related noise refers to the decontamination method by means of temporal signal difference as described by Simpson *et al.* (1987). This techniques allows a decontamination of in-phase acoustic contributions associated with the propagation of the longitudinal or transverse modes at the measurement location. The decontamination was performed using the transducers located at each extremity of the array, which was aligned perpendicular to the flow direction. The 42 mm separation distance between the two spanwise transducers, being about three times the half-height of the test section, ensured that the turbulence contributions were not correlated between the two transducer signals (from S. *et al.* (1987), the minimum distance between sensors to produce a zero cross-correlation is about $\delta/2$ where δ is the shear layer thickness; physically this means that individual large-scaled motions are no move than about δ in spanwise extent). This procedure provided uncontaminated wall-pressure spectra above 20 Hz, at 4.3 m/s, making it possible to observe the maximum of the spectra in the mid-frequency range.

In Figures 4(a)-4(c) the wall-pressure spectra measured at the velocities of 2.3, 3.3 and 4.3 m/s in the reference water flows and in the drag-reducing flows, for different rates of skin friction reduction, are illustrated. The percentages of drag reduction at which the data were taken are indicated in the figure captions. As observed earlier by Kadykov *et al.* (1970), Barker (1973), Greshilov *et al.* (1975), Millward and Lilley (1974), the reduction of the hydrodynamic drag by polymer additives is simultaneously accompanied by a reduction of the spectral levels of the wall-pressure fluctuations. Here, the attenuation effect is observable over the whole frequency range of the wall-pressure spectra. However this attenuating effect is more pronounced in the high frequency range where the wall-pressure contributions are mainly correlated with turbulence activity in the near wall region of the flow. As it can be seen in the spectra, the significant increase of the decay rate at high frequency is associated with a shift of the natural extinction frequency towards a lower value over the whole velocity range. This shift can be attributed to the thickening of the inner region of the boundary layer, in the presence of skin friction reduction, as reported by the numerous investigations on the velocity field concerned by Toms' phenomenon (as a matter of fact, many results of velocity measurements published in the literature indicate a shift of the location of the maximum of turbulence activity toward a greater distance from the wall, which denotes an increase of the extent of the buffer layer. In correlation, a significant decrease of this maximum is observed as well as a reduction of the mean velocity gradient which affects the logarithmic law by increasing its constant term proportionally to the skin friction reduction). Moreover, as previously mentioned by G. *et al.* (1975), the influence of Toms' effect on the wall-pressure spectral feature is found to depend strongly on the flow velocity. This trend appears in the frequency range where the reduction of the spectral level is especially pronounced, as shown in Figure 5. For example, this reduction is about 8 dB at 600 Hz at the velocity of 2.3 m/s, while it only reaches a value of 3.5 dB at 3.3 m/s, and 1.75 dB at 4.3 m/s, for a percentage of drag reduction estimated as 40% in all cases. Hence the intimate relationship between the wall shear stress and the intensity of the wall-pressure fluctuations is unequivocally demonstrated since increasing amounts of drag reduction are associated with a decrease of the integral over the measured spectra.

In order to examine the effect of skin friction reduction on the spectral regions of the wall-pressure field, the wall-pressure spectra were scaled using different sets of flow variables. Since the decontamination procedure could not suppress the facility-related noise below 20 Hz, our analysis is focused on the mid-frequency range (identified approximately as $5 \leq \omega\delta/u_\tau \leq 0.3\,\mathrm{Re}_\tau$ for the turbulent boundary layer) over which the data are found to collapse to a universal scaling law when normalized using the outer flow variables τ_w, u_τ, and δ in the form

$$\Phi(\omega)u_\tau/\tau_w^2\delta \quad vs \quad \omega\delta/u_\tau \tag{2}$$

Note that in a classical turbulent boundary layer flow the maximum for the spectra is obtained in this mid-frequency portion at the approximate value of $\omega\delta/u_\tau \approx 50$.

In addition, the dependence of the spectral levels on the external variables U_b and δ was regarded by scaling the data using the reduced parameters $q = 1/2\rho U_b^2$ and $2\delta/U_b$.

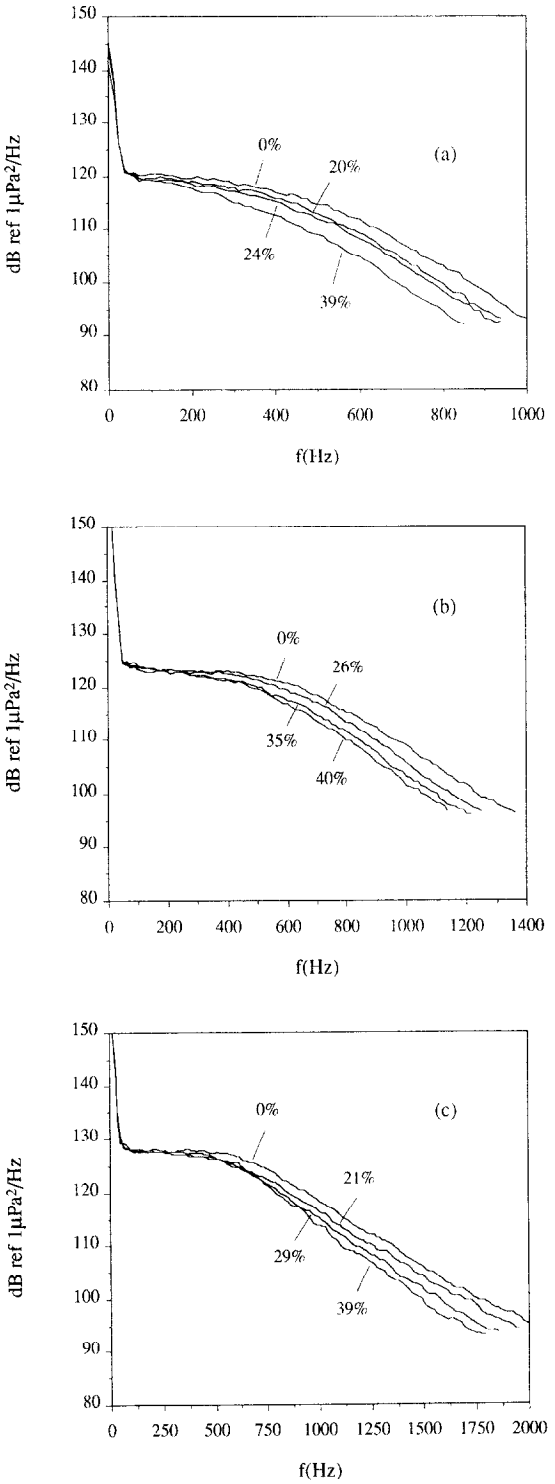

Fig. 4(a)-(c). – Wall-pressure spectra measured in the water flow and in the drag-reducing flows of polyacrylamides for increasing rates of skin friction reduction: (a) 2.3 m/s, (b) 3.3 m/s, (c) 4.3 m/s.

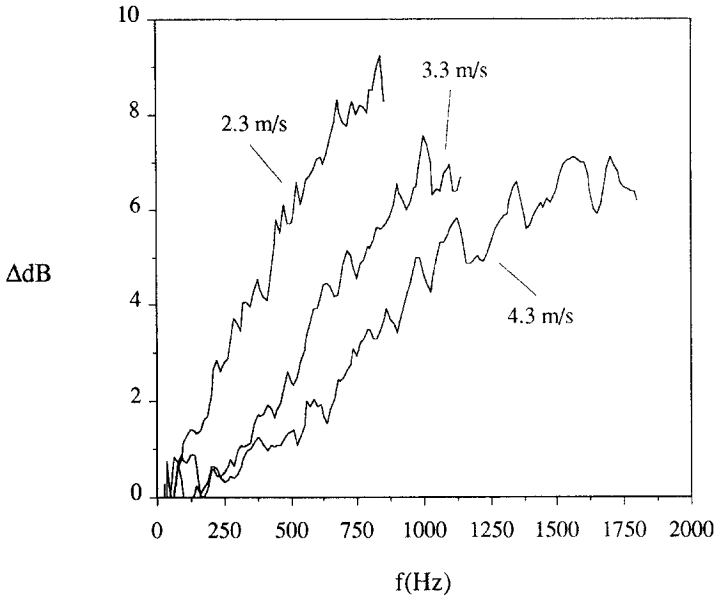

Fig. 5. – Reduction of wall-pressure fluctuation spectral levels at different flow velocities for a constant rate of skin friction reduction. DR% $\approx$ 40%.

Finally, for the lower velocities of 2.3 and 3.3 m/s, the scaling behaviour of the spectra was examined in the high frequency range where the pressure field is governed by an universal scaling law based on the inner flow variables ν, τ_w and u_τ, expressed as

$$\Phi(\omega)u_\tau^2/\tau_w^2\nu \quad vs \quad \omega\nu/u_\tau^2 \tag{3}$$

In Figures 6(a)-6(c) the wall-pressure spectra measured at 2.3, 3.3 and 4.3 m/s in the water flows, were normalized using the respective scaling factors convenient for the different spectral regions. Here, the data were not corrected for the effect of the sensor dimension and the angular frequency spectrum is defined as $\Phi(\omega) = \Phi(f)/4\pi$, where $\Phi(f)$ is the single-sided autospectral density of the fluctuating wall-pressure directly measured.

More particularly, the Figure 6(a) illustrates the wall-pressure spectra normalized using the set of outer variables $q = 1/2\rho U_b^2$ and $2\delta/U_b$ expressed as $\Phi(\omega)U_b/q^2 2\delta$. Although this scaling does not permit any conclusion from the apparent collapse of the spectra in the mid-frequency region (the effects of Reynolds number are not taken into account in this last representation), it provides a comparison of the present measurements to those of G. *et al.* (1975) taken in a comparable flow geometry. Note on that count that a reason for the difference between the spectral levels as well as the frequency extents in the measurements can be attributed to the effect of sensor resolution (R_T (G. *et al.*, 1975) = 0.75 mm). Since the dynamics of the pressure field are essentially governed by the activity of sources located in the inner layer, in the frequency range where the spectra exhibit their drop off, this scaling does not collapse the data in the overlap region as well as the high frequency region of the spectra.

In Figure 6(b), the wall-pressure spectra have been normalized using the outer variables u_τ and δ, for scaling the spectra in the mid-frequency region. As previously observed

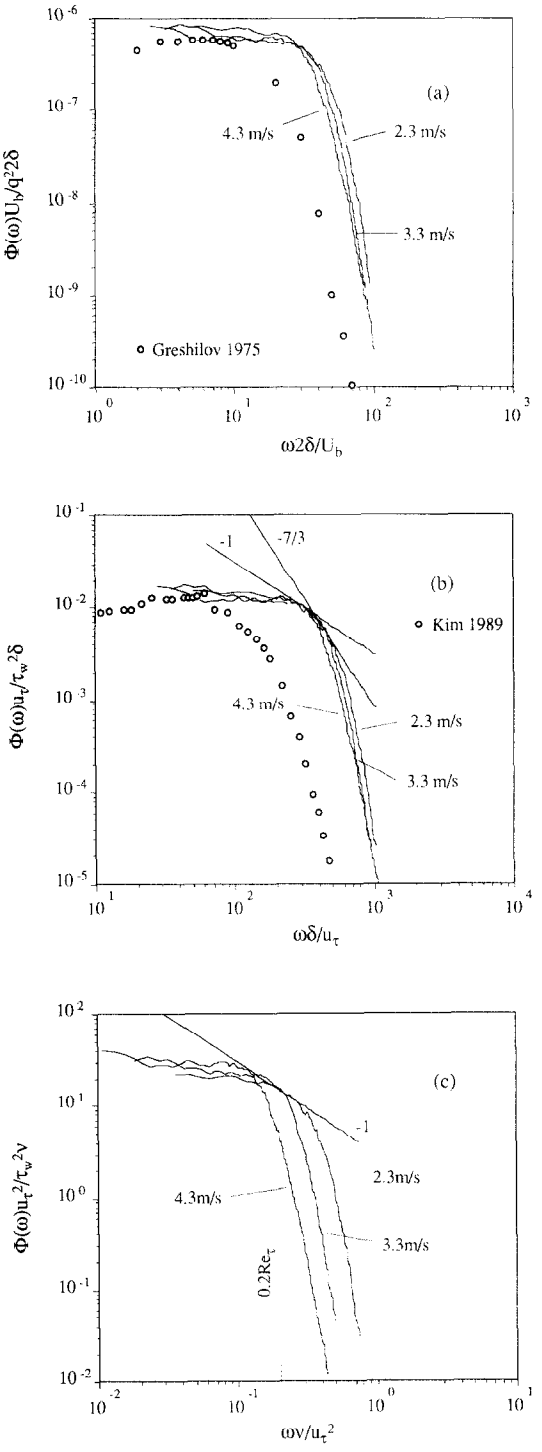

Fig. 6(a)-(c). – Nondimensional wall-pressure spectra measured in the water flows at different velocities: (a) outer variable scaling using q and δ, (b) outer variable scaling using u_τ and δ, (c) inner variable scaling.

by F. and C., 1991, the spectra are found to collapse to a universal scaling law in the approximately frequency range $\omega\delta/u_\tau \leq 0.2\,\mathrm{Re}_\tau$, indicating that the velocity scale u_τ should be an appropriate scale for both the inner and the outer flow structures. For the present data, the maximum of the spectra was not obtained in so far as its position lies in the frequency range where the spectra are contaminated. However, the location of this maximum value was obtained by performing the noise cancellation procedure on the data taken at 4.3 m/s, as is shown later in this section. In the upper part of the mid-frequency region, the spectra are found to exhibit a limited ω^{-1} scaling region which is relevant to the pressure source activity in the logarithmic law region of the flow. As discussed by P. and L., 1974, this overlap region is strongly dependent on the Reynolds number Re_τ of the flow. This trend is shown in the wall-pressure spectra by the increase of the spectral extent of the ω^{-1} scaling region, towards the high frequency range, with increasing flow velocities. In particular, the spectral extent of the -1 slope scaling behaviour can be identified as the reduced frequency range $220 \leq \omega\delta/u_\tau \leq 0.2\,\mathrm{Re}_\tau$ in the present measurements. Note that some reservations should be made about the accuracy of the slopes as well as frequency ranges discussed in our measurements since the effects of transducer mounting could induce deviations on the data in the high frequency region. Concerning this point, Figure 6(b) also displays the power spectrum computed by Kim (1989) from a direct numerical simulation of the pressure fluctuations in a turbulent channel flow. Because of the low Reynolds number considered in the calculation, it is difficult to see the power law behaviour distinctly for the different frequency ranges. We can however observe an apparent collapse of the computation and our results in the lower part of the mid-frequency region.

From the comparison of the scaling effect using the outer variables, and the viscous scales, on the collapse of the spectra, it appears clearly that both the outer and the inner scaling laws hold in the overlap region. This can be seen in Figure 6(b) and 6(c) where the spectra have been scaled using the variables u_τ and δ, and ν, τ_w and u_τ, as expressed in the forms (2) and (3), respectively.

Finally, in Figure 6(c), the reference spectra are shown normalized using inner flow variables ν, τ_w and u_τ. Here it appears that the inner variable scaling provides the universal collapse of the wall-pressure spectra in the upper part of the overlap region delineated by $240 \leq \omega\delta/u_\tau \leq 0.2\,\mathrm{Re}_\tau$ (in our measurements) as well as in the high frequency range for the flow velocities 2.3 and 3.3 m/s. The collapse of the spectra in the high frequency range can not be observed at 4.3 m/s since the reduced cut off frequency of the sensor is less than $\omega\delta/u_\tau = 0.2\,\mathrm{Re}_\tau$. In the high frequency range $(\omega\delta/u_\tau \geq 0.2\,\mathrm{Re}_\tau)$, restricted to the portion where the data are not spatially averaged, the rapid decrease of the spectra is found to follow an approximate $\omega^{-7/3}$ decay rate as observed by several authors in the case of turbulent boundary layer flow. Notably, for reduced frequencies greater than $\omega\delta/u_\tau \approx 610$, the deviation of the spectra from the universal scaling behaviour is attributable to the spatial averaging effect of the sensor.

In Figures 7(a)-7(c), the equivalent wall-pressure spectra measured in the presence of drag reduction have been normalized using the same sets of variables as used for the reference water flows. The spectra presented here were measured at 2.3, 3.3 and 4.3 m/s

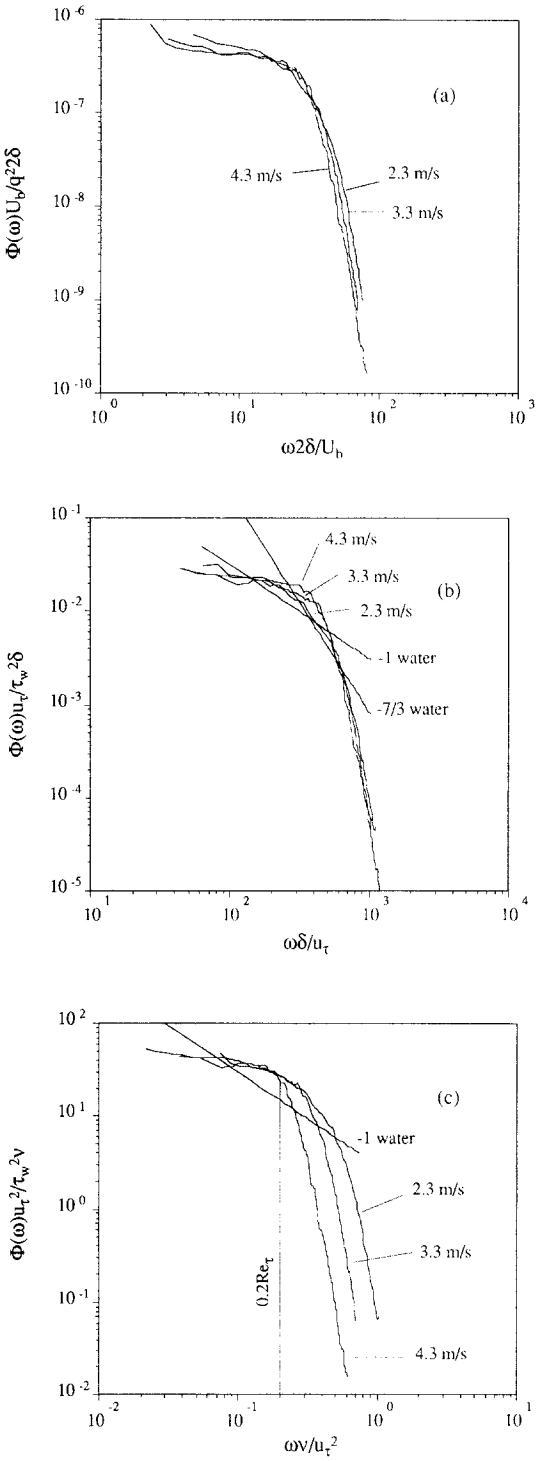

Fig. 7(a)-(c). – Nondimensional wall-pressure spectra measured at different velocities in the drag-reducing flows for a constant rate of skin friction reduction: (a) outer variable scaling using q and δ, (b) outer variable scaling using u_τ and δ, (c) inner variable scaling. DR% $\approx$ 40%.

for a percentage of drag reduction approximately equal to 40% in all cases. Since the concentration of polymers in the drag-reducing flows never exceeded a value of 20 wppm, the apparent viscosity of the fluid was assumed to remain equal to the water dynamic viscosity. An interesting observation that can be drawn from the results is that the spectra measured at different velocities do not exhibit the same scaling behaviour, when compared to the reference flows. As a matter of fact, the spectra displayed in Figure 7(b) appear to collapse in the mid-frequency range, expressed by $\omega\delta/u_\tau \leq 0.2\,\mathrm{Re}_\tau$, on a scaling law that follows a lower decay rate than for the water flows. This tendency seems to be in agreement with the pressure measurement results reported by M. and L., 1974, for drag-reducing flows of Polyox WSR 301 and Separan AP30, at varying concentrations, in a circular pipe. Note that the lack of similitude that can be observed above $\omega\delta/u_\tau \approx 220$ concerns values of the reduced frequency greater than $0.2\,\mathrm{Re}_\tau$ where the outer scaling is not expected to hold. This is supported in Figure 7(c) by the apparent collapse of the upper part of the mid-frequency portion as well as the high frequency region of the spectra (below the sensor cutoff frequency) when scaled using the inner variables. The fact that the spectra exhibit the similar scaling regions as observed for pure water flows indicates that the universal character of turbulence still characterises the drag-reducing flow properties (this is supported by the results of the numerous investigations on the influence of Toms' effect on the instantaneous velocity field published in the literature). However the deviation of the scaling behaviour from the ω^{-1} law obtained in the overlap region implies a modification of the inertial region dynamics owing to the action of the additives on the fine turbulence structures located in the inner layer. Moreover, if we compare the effect of the different scalings on the spectral level, it appears that the spectra measured in the presence of drag reduction experience a shift toward a lower or a higher mean level depending on the type of scaling used. In particular, the spectra normalized using the outer variables q and $2\delta/U_b$ lies well below their equivalents measured in the reference flows, indicating a decrease of the ratio p_{rms}/q in drag-reducing flows. On the other hand, the use of the inner variables for scaling the data shows an increase of the overall spectral level above the average level of the spectra measured in the water flows. This trend conveys an increase of the ratio p_{rms}/τ_w in the presence of Toms' effect. These tendencies can be observed more obviously in Figures 8(a)-8(c) where the normalized spectra, measured at 2.3 m/s in the reference flow and in the drag reducing flows for increasing rates of drag reduction, are displayed.

Since the effect of sensor resolution (as well as transducer mounting) is less prejudicial in the high frequency range at low velocity, the scaling behaviour of the spectra as well as their spectral extent was also examined more particularly at this flow velocity. As mentioned before, the wall-pressure spectra measured in the presence of drag reduction appear to exhibit an overlap region with a scaling behaviour that follows a lower decay rate than in the water flow. Note that in Figure 8(a) the spectra do not collapse on a universal law since they were measured at different percentages of drag reduction. Furthermore, the rapid decrease which characterises the high-frequency region also appears to follow a lower decay rate when Toms' effect occurs as compared to the approximately –7/3 slope obtained for water flows. In addition, examination of the frequency limits for which the mid- and high frequency scaling variables collapse the data indicates a decrease of the

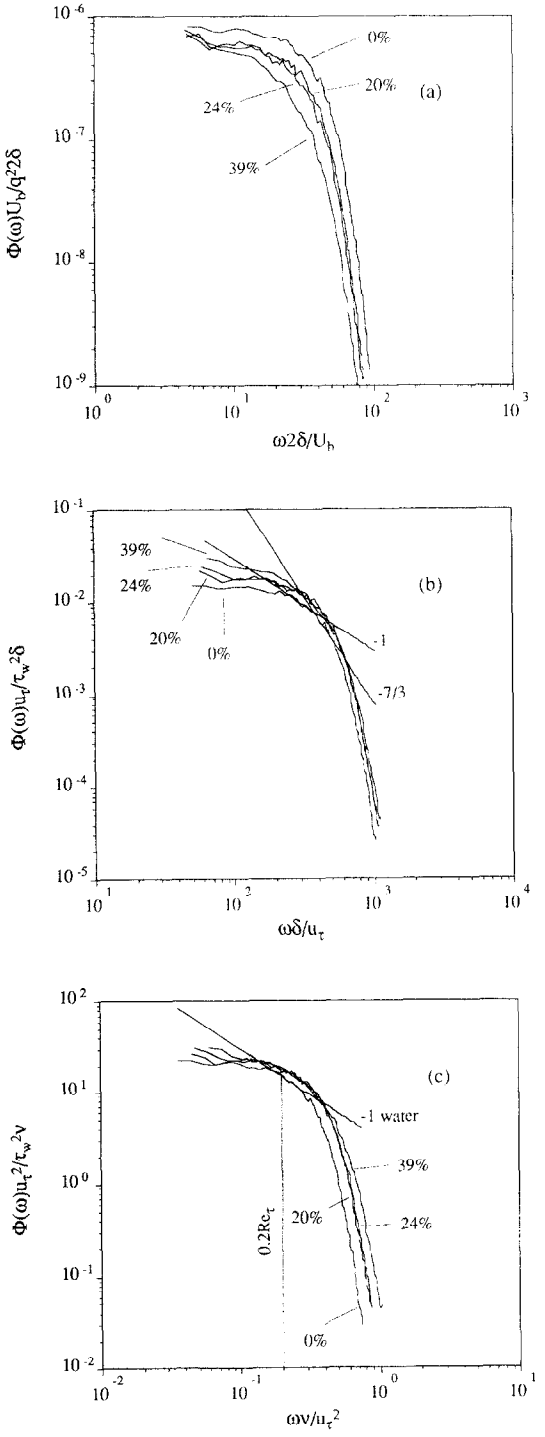

Fig. 8(a)-(c). – Nondimensional wall-pressure spectra measured at 2.3 m/s in the water flow and in the drag-reducing flows for increasing rates of skin friction reduction: (a) outer variable scaling using q and δ, (b) outer variable scaling using u_τ and δ, (c) inner variable scaling.

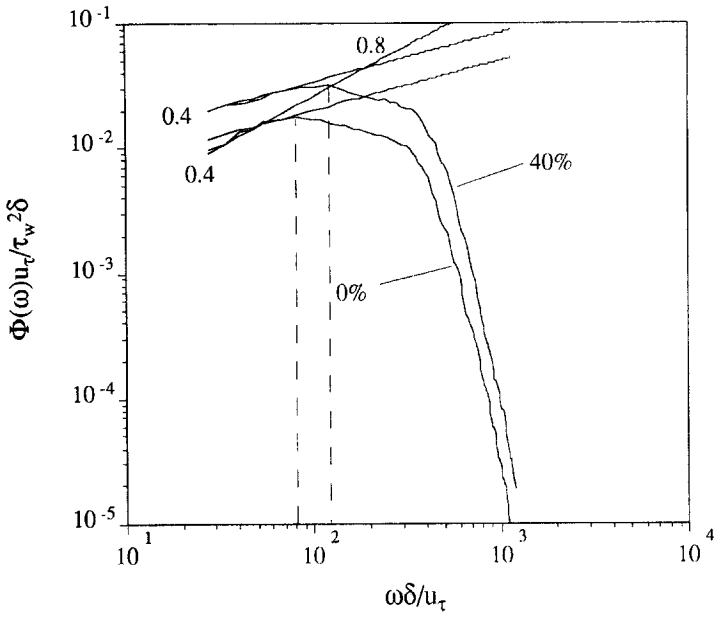

Fig. 9. – Nondimensional wall-pressure spectra measured at 4.3 m/s in the water flow and in a drag-reducing flow for DR% $\approx$ 40% using the noise cancellation procedure. Outer variable scaling using u_τ and δ.

spectral extent of the overlap region corresponding to the thickening of the inner layer induced by the skin friction reduction.

Finally, the effect of the additives on the low frequency range was examined on the uncontaminated spectra measured at 4.3 m/s. These spectra are shown in Figure 9 when normalized using the outer variable scaling based on τ_w, u_τ, and δ as expressed in (2). In the low frequency part of the mid-frequency region identified approximately as $15 \leq \omega\delta/u_\tau \leq 50$, the spectrum measured in the water flow is found to exhibit an approximately $\omega^{0.8}$ behaviour. This scaling behaviour varies slightly, above this frequency range, within the spectral extent $50 \leq \omega\delta/u_\tau \leq 80$, where the scaling law appears to follow a $\omega^{0.4}$ dependence. Note that the scaling behaviour of the spectra could not be observed below the reduced frequency $\omega\delta/u_\tau \approx 15$ since the facility-related noise could not be cancelled in this frequency range. As clearly appears in the figure, the water reference spectrum reaches its maximum value in the mid-frequency range. The value of the reduced frequency at which this maximum occurs is found to be $\omega\delta/u_\tau \approx 80$ for the present data. Such a value is more than the typical value of about 50 mentioned in the literature for the case of the turbulent boundary layer. When Toms' phenomenon occurs, the effect of drag reduction on the low frequency portion of the spectrum appears to increase the spectral extent of the scaling region where the $\omega^{0.4}$ dependence is observed. The increase of this region is connected with a shift of the maximum value of the spectrum towards a higher value of the reduced frequency. In particular, for a percentage of drag reduction estimated as 40% in the present case, this peak is located approximately at the reduced frequency of $\omega\delta/u_\tau \approx 105$.

3.2. Cross-spectral features of wall-pressure fluctuations

3.2.1. *Coherence functions*

Additional information concerning the effect of drag reduction on the spectral feature of the wall-pressure fluctuations was provided by estimating the cross-spectrum. The cross-spectral measurements were obtained without applying the noise cancellation technique to the data although such a technique has been developed in the literature. The cross-spectra were measured using both streamwise and spanwise sensor spacings at the flow velocities of 2.3, 3.3 and 4.3 m/s. Phase unwrapping and frequency smoothing was performed on the data in order to obtain the results presented in this section. From the set of separation distances which characterize the locations of the pinhole transducers, dimensionless spacings ξ/δ could be provided within the range $0.4 \leq \xi/\delta \leq 2.8$ (ξ denotes the separation distance between two pinhole sensors). Note that since the wall-pressure fluctuations suffer a strong decrease of the lateral correlation over distances greater than $\delta/2$, the measurements concerning spanwise spacings were obtained using the minimal separation distance of 0.4 δ.

In Figures 10(a) and 10(b), the respective streamwise coherence spectra measured at the velocity of 4.3 m/s in the reference flows, and in the presence of drag reduction, are illustrated. The percentage of drag reduction at which the data were taken, when Toms' effect occurs, is about 40% in the present case. Here, only data obtained at 4.3 m/s are shown since similar trends could be observed at the velocity of 2.3 and 3.3 m/s. Moreover, the contamination of the measurements by the low frequency vibro-acoustic contributions is more attenuated for large values of ξ/δ with increasing velocities.

As observed by several authors, the coherence functions measured in the water flow are found to collapse on a universal curve at high frequency for all separation distances. From Figure 10(b), this universal decay also appears to characterize the cross-spectra measured in the presence of skin friction reduction. In the figures, the reference curves plotted as a dashed line have been computed from the theoretical formulation of the coherence spectra as expressed by Corcos (1964). The decay rate of the exponential form, empirically estimated for the present data, has an approximately constant value of 0.135 in the both case of water flow and of drag-reducing flow, and is lower than the typical decay rates of 0.18-0.22 obtained by several authors for fully developed turbulent pipe flows (Horne, 1990). Such a value for the decay rate indicates that the wall pressure sources lose their identity in travelling a distance of approximately three wavelenths.

In the low frequency region, a rapid loss of coherence is observed over the entire range of separation distances. This lack of similarity scaling conveys the physical impossibility for the low frequency components to be correlated over long streamwise distances. This would indeed require that the wall pressure source convect over equally long distance without being distorted by the mean gradient and the turbulence activity.

When comparing the low frequency regions of the streamwise coherence functions measured in the pure water flow and in the presence of additives, it appears unambiguously that a more pronounced loss of coherence characterises the low frequency range when Toms' phenomenon occurs. As illustrated in Figures 11(a) and 11(b), where the coherence

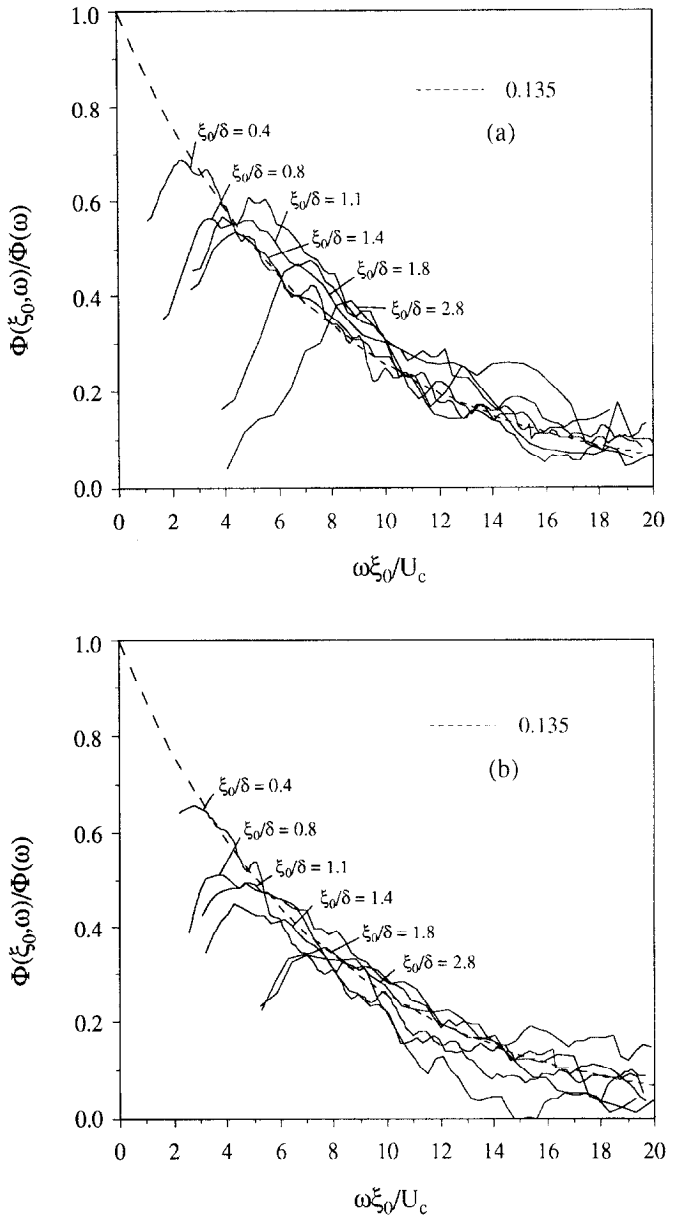

Fig. 10(a)-(b). – Streamwise coherence spectra *versus* cross-spectral phase $\omega\xi_0/U_c$ for a range of spacings $0.4 \leq \xi_0/\delta \leq 2.8$: (a) water flow at 4.3 m/s, (b) drag-reducing flow at 4.3 m/s for DR% $\approx$ 40%. Dashed line is for Corcos' formulation of coherence spectra using a 0.135 decay rate.

data were obtained using fixed ξ, this deviation from the similarity scaling (which implies an increase of the distortion of the low frequency pressure source by the turbulent motions), concerns values of $\omega\delta/U_c$ located below the peak that occurs in the coherence spectra. In particular, the coherence functions obtain this peak at approximately $\omega\delta/U_c \approx 5.3$ for the smallest spacing, $\xi = 0.4\,\delta$, and at $\omega\delta/U_c \approx 2.4$ for the largest one estimated as $\xi = 2.8\,\delta$, in the water flow. The corresponding values of $\omega\delta/U_c$ at

which the coherence spectra show a peak are about 6.1 and 2.8 for the smallest and the largest spacings, respectively, in the case of drag reduction. Hence, the shift of the peak location towards a higher value of the reduced frequency obtained in case of Toms' phenomenon indicates clearly the more significant decorrelation of the low frequency pressure source in the drag-reducing flow.

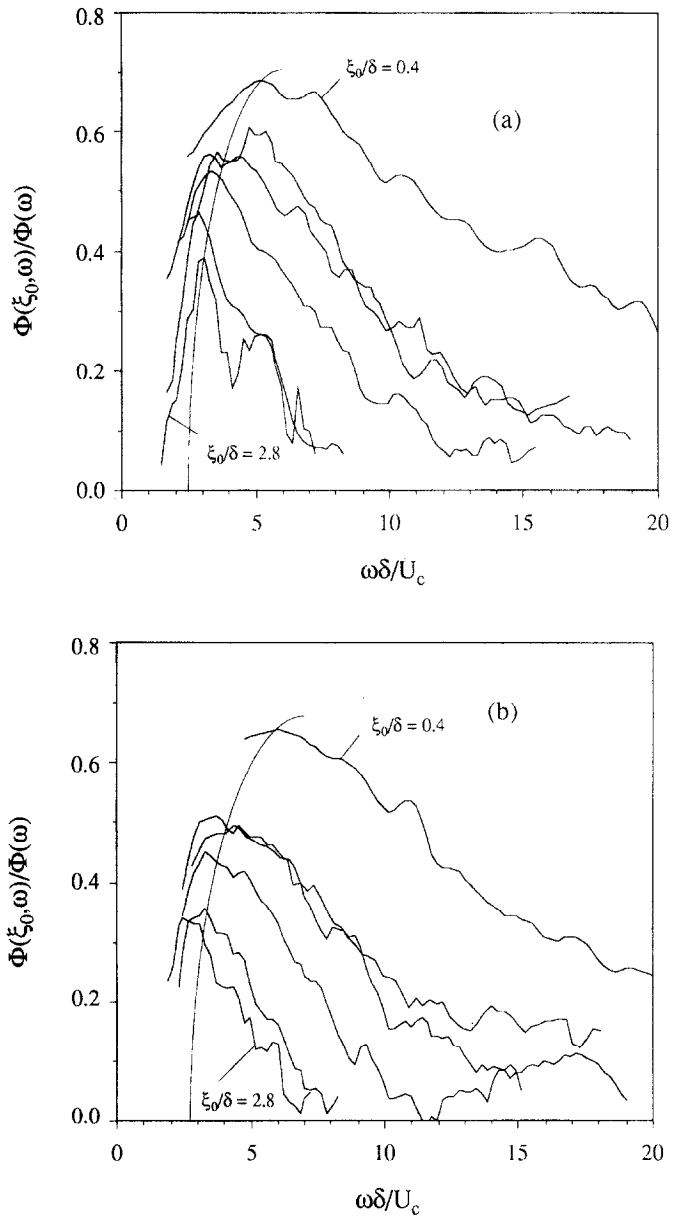

Fig. 11(a)-(b). – Streamwise coherence functions *versus* dimensionless frequency $\omega\delta/U_c$ for a range of spacings $0.4 \leq \xi_0/\delta \leq 2.8$: (a) water flow at 4.3 m/s, (b) drag-reducing flow at 4.3 m/s for DR% $\approx$ 40%.

In Figures 12(a)-12(b), similar coherence spectra have been displayed as a function of the phase $\omega\xi/U_c$ at fixed values of the angular frequency. Such a display provides information on the spatial decay that fixed wave number components experience as the pressure field convects downstream. Here the coherence spectra measured in the water flow have been plotted for values of the dimensionless frequency over the range

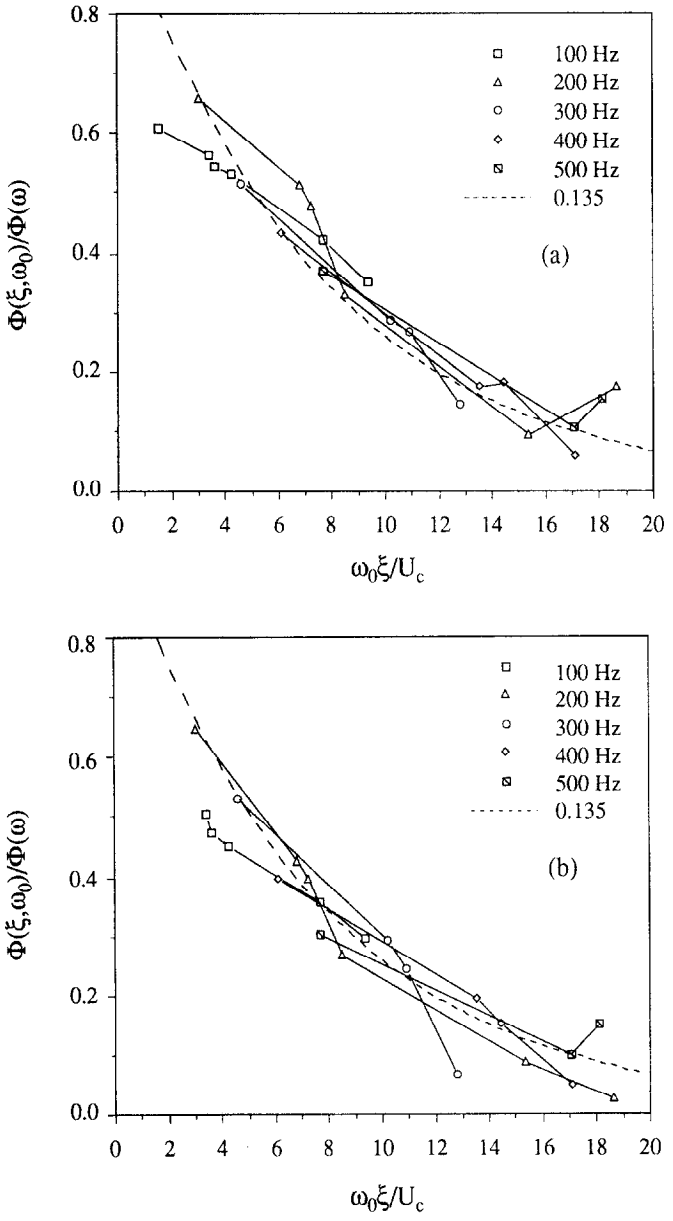

Fig. 12(a)-(b). – Streamwise coherence functions *versus* cross-spectral phase $\omega_0\xi/U_c$ for a range of frequencies: (a) water flow at 4.3 m/s, (b) drag-reducing flow at 4.3 m/s for DR% $\approx$ 40%. Dashed line is for Corcos' formulation of coherence spectra using a 0.135 decay rate.

$55 \leq \omega\delta/u_\tau \leq 276$. The equivalent frequency range corresponding to the coherence spectra measured in the presence of skin friction reduction is $69 \leq \omega\delta/u_\tau \leq 348$. As expected for the higher values of fixed frequency the spectra are found to collapse to a similarity scaling behaviour which follows an exponential decay rate similar to that previously estimated. On the other hand, the spectra deviate from the similarity scaling law for the lower values of the fixed frequency in both cases of water flow and drag-reducing flow. This deviation implies a higher decay rate of the low wave number contributions which also appears to be more pronounced when Toms' effect occurs.

From the overall measurements of the streamwise cross-spectral characteristics taken for water flows and drag-reducing flows, it can be inferred that the high wave number components experience the same amount of decay as they are convected downstream. This decay rate is found to be comparable in the reference flow and in the presence of skin friction reduction. At low values of the wave number, the coherence functions exhibit a peak which can be identified as an approximate measure of the lower limit for which similarity scaling no longer holds. Such a behaviour is related to the high pass filtering character of the turbulent boundary layer. In the presence of Toms' phenomenon, the value of this cut-off frequency is increased as shown in the data by the more pronounced deviation of the cross spectra from the universal scaling behaviour at low values of the dimensionless frequency $\omega\delta/U_c$. Moreover, the pronounced deviation from the similarity scaling which accompagnies the skin friction reduction should be correlated to the shift of the maximum of the autospectrum towards a higher value, as observed when scaling the data using δ/u_τ. As a matter of fact, the value of the cut-off frequency lies within a range which is approximately the same dimensionless frequency for which the frequency spectrum reaches its maximum value. In particular, the cut-off frequency obtained in the reference flow, for the overall separation distances, is found to lie within the reduced frequency range $41 \leq \omega\delta/u_\tau \leq 90$ and its corresponding value, measured in the drag-reducing flow, is located in the interval $57 \leq \omega\delta/u_\tau \leq 125$.

Finally, the equivalent measurements of the lateral coherence function, estimated using the 0.4 δ spanwise separation distance, are shown in Figure 13. The theoretical curve plotted on the figure was computed from the Corcos (1964) formulation of the coherence spectra. The constant decay rate in the spanwise direction is found to be about 0.7 which is the value currently obtained for turbulent boundary layer flows. The direct comparison of the coherence functions, measured in the pure water flow and in the drag reducing flow, indicates that a correlated increase of the spanwise coherence function occurs in the presence of skin friction reduction. This trend seems to affect the whole range of the cross-spectral phase $\omega\xi/U_c$, implying an increase of the large pressure source lateral anisotropy.

3.2.2. *Convection velocity*

Other aspects of the effect of drag reduction on the wall-pressure were also obtained by examining the streamwise convection velocity of the pressure fluctuations. The convection velocity was estimated by inverting the phase function of the cross-spectrum using the identity $\alpha(\xi,\omega) = -\omega\xi/U_c$. As for the coherence function measurements, the data were

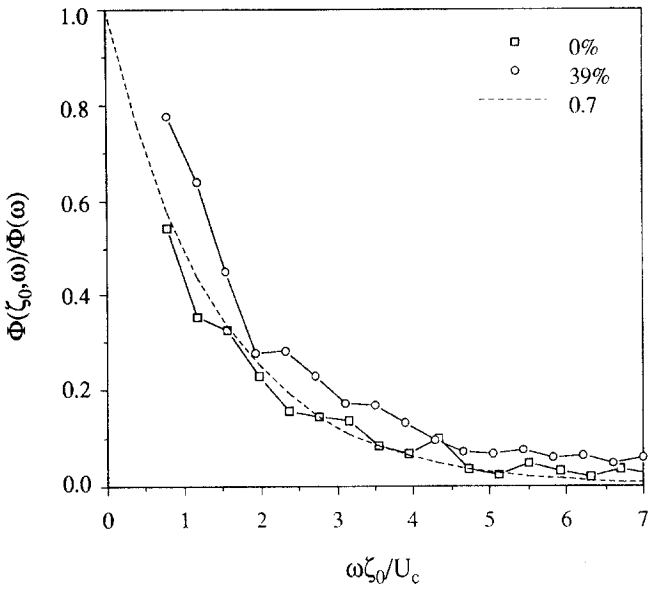

Fig. 13. – Spanwise coherence spectra *versus* cross-spectral phase $\omega\xi_0/U_c$ (ξ_0 = 6 mm) measured at 4.3 m/s in the water flow and a the drag-reducing flow for DR% $\approx$ 40%.

taken over a set of dimensionless spacings ξ/δ ranging from 0.4 to 2.8. In Figures 14(a)-14(b) the convection velocities measured in the reference flow and in the presence of Toms' effect for DR% $\approx$ 40%, are expressed as functions of the frequency parameter $\omega\delta/u_\tau$. In both cases, it appears that the convection velocity presents a peak which is located at an approximately constant value of the argument $\omega\delta/u_\tau$ over the range of different spacings. This peak of convection velocity is found to occur at $\omega\delta/u_\tau \approx 70$ in the reference flow, whereas its equivalent for the drag-reducing flow is shifted towards a higher value of the reduced frequency, approximately equal to $\omega\delta/u_\tau \approx 110$. If we compare the location of the peak of convection velocity and the position of the maximum in the wall-pressure spectra, for both case of water flow and drag-reducing flow, it can be seen that they lie at comparable value of $\omega\delta/u_\tau$. This suggests that not only are the lowest wave numbers below the wave number cut-off location severely attenuated, but they also convect at the lower overall velocity.

Another interesting characteristic of the effect of Toms' phenomenon on the convection velocity is obtained when looking at the relative position of the curves measured at fixed ξ/δ. In particular, the peak value of the ratio $U_c(\xi,\omega)/U_0$, measured in the drag reducing flow, is found to be less than its corresponding value in the reference flow, for spacings $\xi/\delta < 1$. On the other hand, this peak reaches a higher value, in the presence of skin friction reduction, on the curves established using spacings larger than $\xi/\delta \sim 1$. This trend is confirmed in Figures 15(a) and 15(b) where the ratio $U_c(\xi, \omega)/U_0$ is displayed against ξ/δ for fixed values of the frequency. Here, not only do the peak values appear to undergo this scattering but this effect is observable over a broad frequency range. This influence of the drag reduction on the convection velocity can be explained in so far as the convection velocity can be assumed to equate to the value of the mean flow

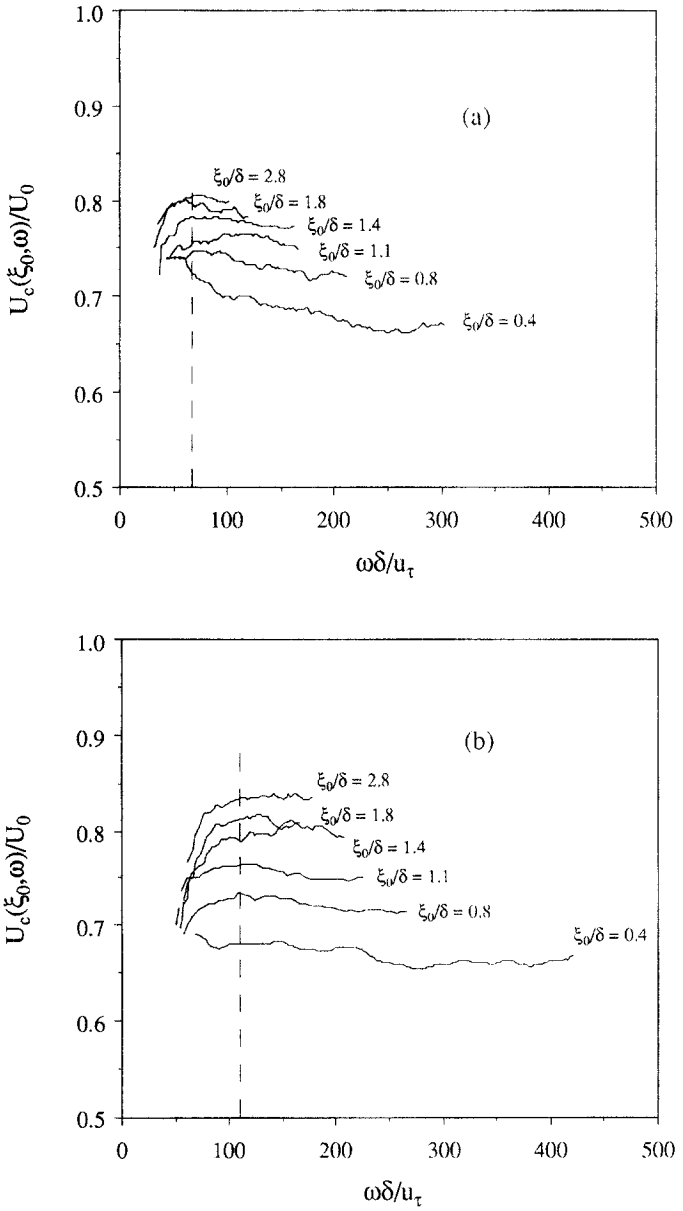

Fig. 14(a)-(b). – Convection velocity *versus* reduced frequency $\omega\delta/u_\tau$ for a range of spacings $0.4 \leq \xi_0/\delta \leq 2.8$: (a) water flow at 4.3 m/s, (b) drag-reducing flow at 4.3 m/s for DR% $\approx$ 40%.

velocity at the pressure source location. As a matter of fact, the range of ξ/δ over which the convection velocity is found to experience a relative decrease will be concerned with pressure sources located within the range of distances "y" normal to the wall where the drag reduction induces a decrease of the mean velocity gradient. The defect of mass flow rate in the wall region (owing to the decrease of the mean velocity) being balanced by an increase of the mean velocity in the core region of the flow (in order to maintain the

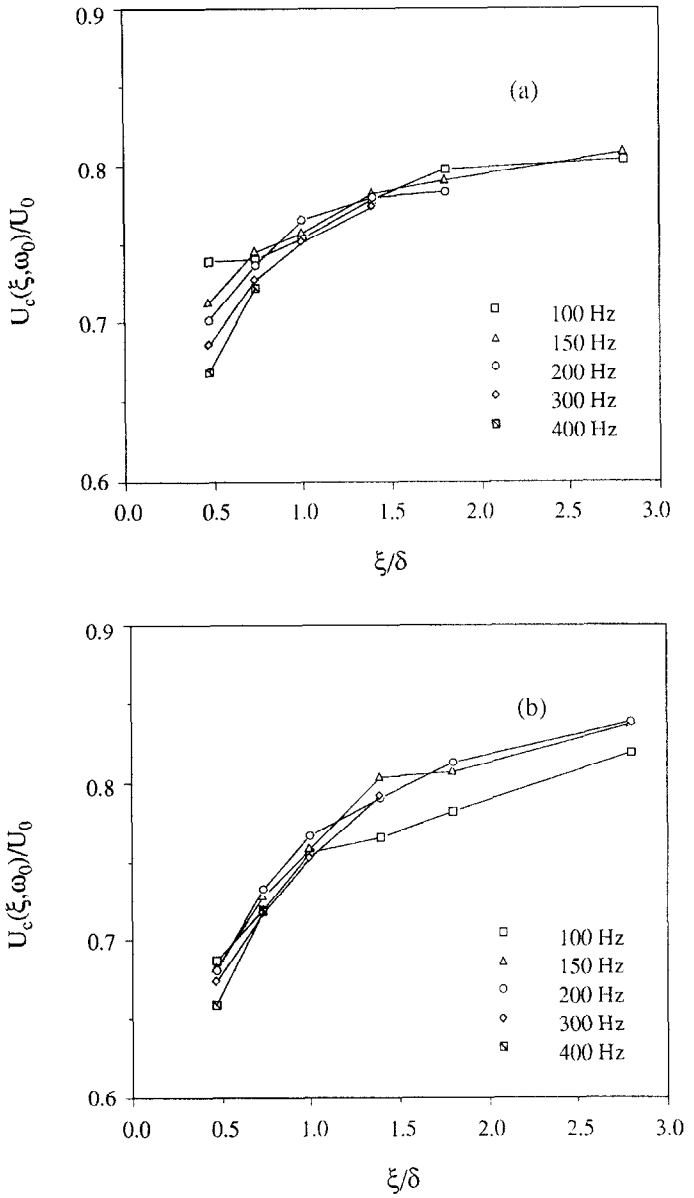

Fig. 15(a)-(b). – Convection velocity *versus* streamwise spacing ξ/δ for a range of frequencies: (a) water flow at 4.3 m/s, (b) drag-reducing flow at 4.3 m/s for DR% $\approx$ 40%.

total mass rate) the range ξ/δ over which the ratio $U_c(\xi,\omega)/U_0$ is relatively increased should relate to contributions of pressure sources located in the centrepart of the flow.

3.3. Root mean square of pressure fluctuations

The root mean square values of the wall-pressure fluctuations were estimated by numerically integrating the frequency spectra obtained without performing the noise

cancellation procedure. The integration was computed from 50 Hz (since the vibro-acoustic contamination from the facility was below this frequency) to the upper frequency limit of response of the pinhole sensor used to measure the wall-pressure field. In order to estimate the error induced by limiting the integration in the low frequency range, the rms value of the wall-pressure amplitudes was computed assuming that the spectrum follows a $\omega^{0.4}$ scaling (as observed on the decontaminated spectra) in the mid-frequency region, below its maximum value. The comparison of rms pressure amplitudes indicated that the contributions to the rms value, for frequencies less than 50 Hz, is about 4% making our results comparable with those obtained directly from decontaminated data.

Here, it should be noted that the use of pinhole transducers for measuring the wall pressure fluctuations can present some potential problems. In particular, Bull and Thomas (1976) have observed that the discontinuity induced in the wall by the pinhole itself can produce a substantial increase of the high frequency levels of the spectra. On the other hand, F. and C. (1991), and Gedney and Leehey (1989), concluded that the pinhole sensors are effective for wall-pressure measurements. For the present data, the ratio p_{rms}/τ_w estimated in the water flows for different values of the Reynolds number $u_\tau \delta/\nu$ appears to compare favourably to the results obtained in channel or pipe flows, as published in the literature (Horne, 1990).

In so far as the shear velocity is decreased when drag reduction occurs, a difficulty has arisen in comparing the wall-pressure amplitudes, both from an effect of transducer size, and a variation of the Reynolds number Re_τ. A suitable way to avoid these effects would consist of comparing the data at identical wall shear stress for different rates of skin friction reduction, but such a procedure would require extensive measurements at numerous flow rates or hazardous extrapolations that we did not venture upon. In fact, the effect of transducer size, which is expected to overestimate the rms value of the wall-pressure fluctuations, when drag reduction occurs, is attenuated by the correlated shift of the drop off of the spectra towards lower frequencies. Hence, for the purpose of comparing the different results, the data were taken at a constant flow rate and the influence of Toms' phenomenon on the rms values of the wall-pressure fluctuations was regarded with respect to the percentage of drag reduction. In Figures 16(a)-16(b), the evolution of the ratios p_{rms}/τ_w and p_{rms}/q, measured at 2.3, 3.3 and 4.3 m/s, in the water flow and for increasing rates of drag reduction are displayed as functions of DR%, respectively.

For the reference water flows, the values of p_{rms}/τ_w and p_{rms}/q obtained at 2.3, 3.3 and 4.3 m/s are found to be 2.19, 2.24, 2.36 and 0.00774, 0.00749, 0.00722 and compare favourably to the results obtained in channel or pipe flows at similar Reynolds number.

As previously observed for the spectra, clearly it appears that the effect of skin friction reduction is accompanied with an increase of the ratio p_{rms}/τ_w. This trend is unequivocally attributable to the presence of Toms' effect since the value of p_{rms}/τ_w denotes an increasing function of the Reynolds number Re_τ in conventional turbulent boundary layer flows. Moreover, Figure 16(a) shows that the data for this value collapse to a single linear relation to the rate of drag reduction. This feature implies that the velocity scale u_τ should be the more appropriate scale for both the inner and outer flow

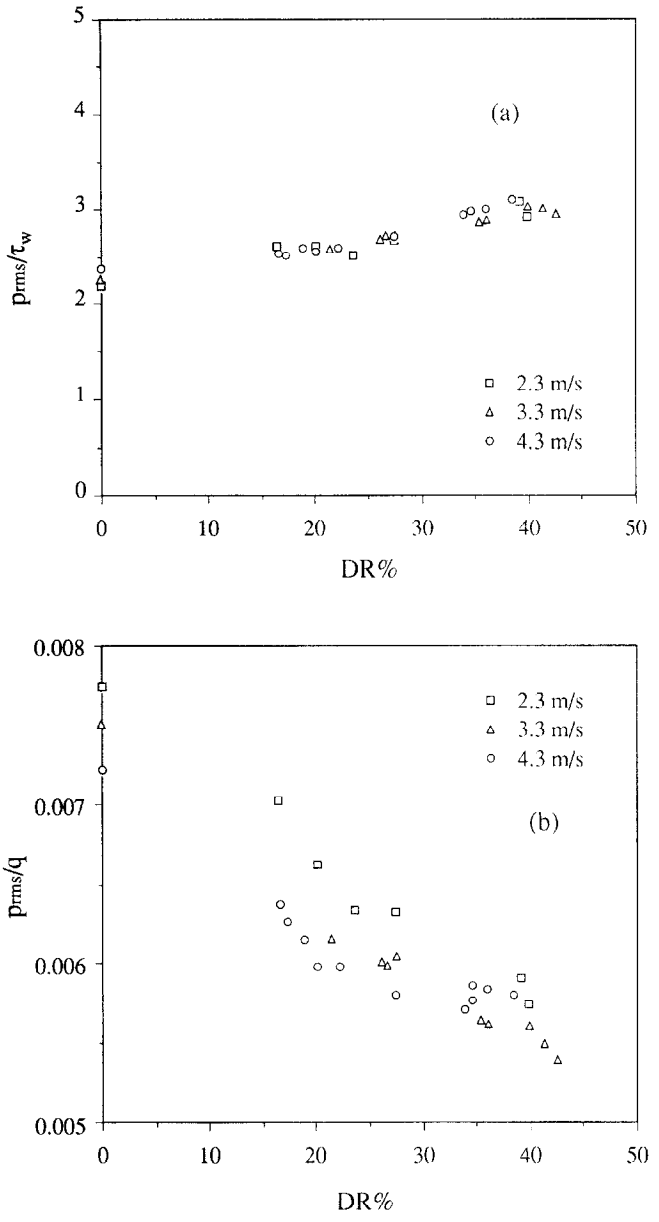

Fig. 16(a)-(b). – Variations in the normalized rms wall-pressure as a function of skin friction reduction: (a) normalization based on wall shear stress, (b) normalization based on dynamic pressure.

structures, as proposed by P. and L. (1974). On the other hand an opposing tendency is found to characterise the variation of the ratio $p_{\rm rms}/q$ with DR%. This can be seen in Figure 16(b) where the values of $p_{\rm rms}/q$ appear to decrease monotonicaly as the rates of drag reduction are increased. Such behaviour is also unequivocally attributable to the effect of the additives since the ratio $p_{\rm rms}/q$ denotes a decreasing function of the size of the sensor (*see* Schewe, 1983).

Note that similar trends concerning the evolution of $p_{\rm rms}/\tau_w$ and $p_{\rm rms}/q$ in the presence of drag reduction have been reported by G. *et al.* (1975) in drag-reducing flows of polyethylene oxide dilute solutions for drag reduction percentages ranging from 70% to 80%. However, the author did not mention the linear feature of the evolution of the ratio $p_{\rm rms}/\tau_w$ with DR% as obtained in the present results. Concerning this point, we estimate that the linear behaviour observed in the present data should not be extrapolated to higher flow velocities in so far as the efficiency of the additives should affect the high frequency part of the broader frequency band spectra differently.

3.4. Probability density distribution of wall-pressure fluctuations

Further insight into the effect of drag reduction on the statistical properties of wall-pressure fluctuations was obtained by estimating the probability density distribution of the pressure amplitudes. The probability density distributions were computed from the uncontaminated data taken at the flow velocity of 4.3 m/s for increasing drag reduction rates. As mentioned in the latter section, a problem arises in comparing the trend of the data due to the decrease of the dimensionless transducer size, when drag reduction occurs. In addition, the effect of transducer size has a considerable effect on the shape of the probability density distribution, making it difficult to estimate the influence of the skin friction reduction alone on the occurrence of the pressure amplitude in the regions where non Gaussian effects are of special interest. Another error can affect the data by the overestimation of the rms value of the pressure amplitudes owing to the residual facility-related noise. In Figures 17(a)-17(b), the probability density distributions of pressure amplitude measured for increasing drag reduction rates are illustrated. Figure 17(a) shows the probability density distributions obtained over the drag reduction range $0 \leq \mathrm{DR}\% \leq 40\%$ when the pressure amplitudes are related to the dynamic pressure of the flow expressed as $q = 1/2\rho U_0^2$. Here, the probability distributions were normalized in such a way that the area under each curve has the value 1. As can be seen by directly comparing the data, the presence of Toms' phenomenon affects the continuous expansion of the probability distribution as the percentage of drag reduction is increased. In particular, the probability of the occurrence of higher pressure amplitudes decreases as the skin friction reduction becomes more significant whereas the opposite trend is observed for very low pressures amplitudes. This effect is clearly attributable to the influence of the additives since the decrease of the transducer size alone would affect the shape of the probability distributions the opposite way (as observed by S., 1983). Thus, since the higher pressure amplitudes are identified as frequency contributions from the spectral region of decay, the decrease of such occurrences can be connected with less intense activity of pressure sources in the inner region as observed on the spectra measured in the drag-reducing flows. Moreover, the higher amplitudes being found to contribute about 40% to the rms pressure, the decrease of these events is in agreement with the shift of the nondimensional spectra towards a lower level observed for drag-reducing flows when normalized using the outer variables q and $2\delta/U_b$. Figure 17(b) shows the equivalent density probability distributions of the pressure amplitudes related to the rms pressure. As for the curves presented in Figure 17(a), the probability distributions

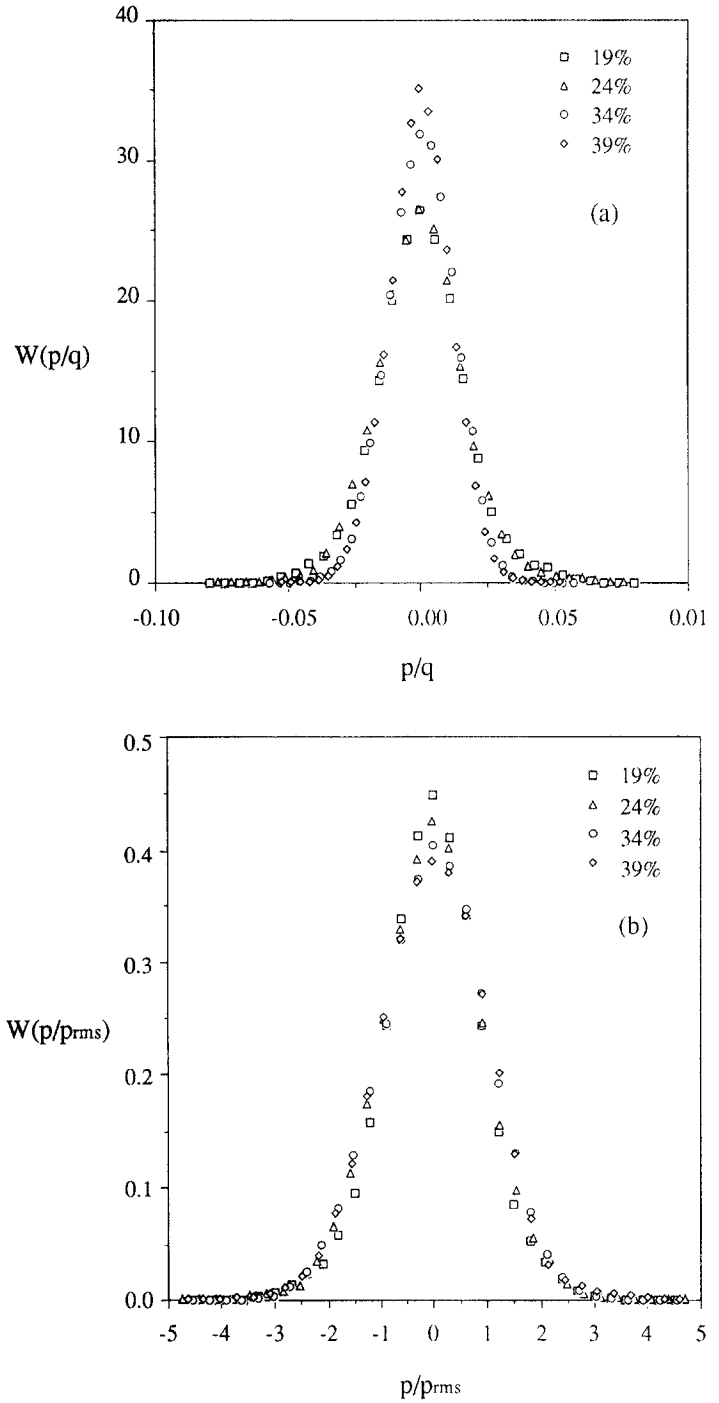

Fig. 17(a)-(b). – Probability density distribution of wall-pressure amplitudes measured in drag-reducing flows for increasing rates of skin friction reduction: (a) normalized to the dynamic pressure, (b) normalized to their corresponding rms value.

were normalized in such a way that their integral over the p/p_{rms} range is unity. For the present data, the shape of the probability distribution measured at the lower rate of drag reduction is comparable to the one obtained by Schewe beneath a zero pressure gradient turbulent boundary layer using transducer sizes within the range $75 \leq d^+ \leq 168$. It seems that the effect of drag reduction is accompanied by a decrease in the occurrence of very low amplitudes contributions and an increase the high amplitude contributions. This opposite trend, when compared to the results displayed in Figure 17(a), is to be related to the decrease of the p_{rms} values in the presence of Toms' effect. Note that it is difficult to attribute the increase of the high pressure amplitude occurrence to the effect of drag reduction alone since the decrease of transducer size connected with the skin friction reduction affects the shape of the probability distributions in the same way.

From the overall results shown in Figures 17(a)-17(b), it can be concluded that the activity of the pressure sources in the buffer region, as well as in the log-law region of the flow, is decreased in drag-reducing flows when compared to a classical turbulent flow at comparable flow rates. On the other hand, this activity appears to be more intense when compared to a conventional fully developed turbulent flow at comparable value of the wall shear stress.

4. Conclusion

The present investigation shows clearly the interest of drag reduction techniques in order to diminish the harmful effects associated with noise generation in the turbulent environment. In particular, this appears eloquently when considering the correlated effect of increasing amounts of drag reduction on the energy of the wall-pressure fluctuations. The examination of the spectral features of the frequency spectrum in the reference flow as well as in the presence of drag reduction is found to support previous investigations concerned with the identification of the turbulent source regions. As a matter of fact, it is observed that the outer and inner variable scaling of the data provide respectively an universal collapse of the spectra measured in the water flows in the mid-frequency region (identified approximately as $100 \leq \omega\delta/u_\tau \leq 0.2\,\mathrm{Re}_\tau$) and in the high frequency range ($\omega\delta/u_\tau \geq 0.2\,\mathrm{Re}_\tau$) over the velocity range studied. Such a collapse is also observed in the spectra in the presence of Toms' effect for data taken at comparable drag reduction rates, but in this case, the effect of drag reduction is found to affect predominantly the spectral extent and the typical decay rate of the overlap region (where the contributions are attributable to the turbulent activity in the log-law region of the flow). Concerning this point, the modification of the overlap region extent might be correlated to the thickening of the buffer layer. Note that a broader range of flow velocities and the use of wave number-phase velocity representation should provide a better insight into the Reynolds number dependence of the pressure spectrum in the overlap region. On the other hand, the change of the decay rates, in the inertial and high frequency zones, can be associated with the reduction of both transverse velocity fluctuations (Reynolds stress) and mean velocity gradient, in the inner region (through the turbulence energetic process), as observed by many authors in the presence of Toms' phenomenon. Thus, this

work supports the fact that the pressure sources which mainly contribute to the energy of the high frequency portion of spectrum are located in the inner layer. On the contrary, it is difficult to draw any conclusion as to whether the first or the second term of the Poisson's equations plays a dominant role. Actually, the drag reduction is expected to affect both of the source terms since the Reynolds stress and the mean velocity gradient experience a significant attenuation. From the decontaminated data, it is shown that the frequency spectrum obtains a maximum in the mid-frequency range approximately at a reduced frequency of 80 for the present results. The location of this maximum is to be correlated with the appearance of a peak in the cross-spectra obtained at fixed frequency as well as in the convection velocity since they are found to occur in comparable ranges of the reduced frequency in both water flows and drag-reducing flows. In particular, these singularities are shifted to a higher value of the reduced frequency which was found to be about 105 in the presence of Toms' effect, for a drag reduction estimated as 40%. This behaviour indicates the existence of a low wave number cutoff effect which delineates a group of low wave numbers associated with large scale contributions and a group of high wave numbers concerned with turbulent sources in the inertial region where eddies decay proportionally to their size. These results also support the fact that turbulence sources in the inner and outer layers contribute to high and mid-frequency ranges, respectively. Moreover this conjecture is confirmed by the convection velocity data under the assumption that the convecting turbulent structures match those of the pressure field.

Finally, examination of the statistical properties of the temporal pressure signals underlines the significant contribution of the high pressure peaks to the integrated power spectral level. As a matter of fact the influence of drag reducion on the probability density distributions is found to affect predominantly the occurrence of the higher amplitude contributions, associated with the appearance of non gaussian effects, both in the positive and negative range.

In so far as the effect of the additives on the turbulence activity is essentially located in the near wall region of the flow, these events can be related to the bursting process as previously inferred by (Schewe, 1983), Haritonidis *et al.* (1990), and Astolfi *et al.* (1992). Notably, this relationship is supported by the reorganisation of the spatial and temporal flow patterns, in the wall vicinity, which accompagnies Toms' effect. In particular, it seems that the significant decrease of the spatially averaged bursting rate, associated with the drag reduction, might be linked with the reduction of the occurrence of large pressure peaks that is observed in the present study.

REFERENCES

ASTOLFI J. A., BALLY P., FAGES A., FORESTIER B. E., 1992, Relation between wall-pressure fluctuations and a large intantaneous velocity gradient $\partial U/\partial y$ beneath a turbulent boundary layer, *Eur. J. Mech., B/Fluids*, **11**, 573-586.

BARKERS S. J., 1973, Radiated noise from turbulent boundary layers in dilute polymer solutions, *Phys. Fluids*, **16**, 1387-1394.

BLAKE W. K., 1970, Turbulent boundary-layer wall-pressure fluctuations on smooth and rough walls, *J. Fluid Mech.*, **44**, 637-660.

BULL M. K., THOMAS S. W., 1976, High frequency wall-pressure fluctuations in turbulent boundary layers, *Phys. Fluids*, **19**, 597-599.

CORCOS G. M., 1963, Resolution of pressure in turbulence, *J. Acoust. Soc. Am.*, **35**, 192-199.

CORCOS G. M., 1964, The structure of the turbulent pressure field in boundary layer flows, *J. Fluid Mech.*, **18**, 353-377.

FARABEE T. M., CASARELLA M. J., 1991, Spectral features of wall pressure fluctuations beneath turbulent boundary layers, *Phys. Fluids A*, **3**, 2410-2420.

GEDNEY C. J., LEEHEY P., 1989, Wall-pressure fluctuations during transition on a flat plate, ASME Procs, Symposium on flow induced noise due to laminar-turbulent transition process, ASME-NCA, **5**.

GRESHILOV E. M., EVTUSHENKO A. V., LYAMSHEV L. M., 1975, Hydrodynamic noise and the Toms' effect, *Sov. Phys. Acoust.*, **21**, 247-251.

HARITONIDIS J. G., GRESKO L. S., BREUER K. S., 1990, Near-Wall Turbulence, Ed Hemisphere (New York), 397-417.

HORNE M., 1990, Physical and computational investigation of the wall-pressure fluctuations in a channel flow, NRL Memorandum report 6628, 87-145.

JOHANSSON A. V., HER J. Y., HARITONIDIS J. H., 1981, On the generation of high-amplitude wall-pressure peaks in turbulent boundary layers and spots, *J. Fluid. Mech.*, **175**, 119-142.

KADYKOV L. F., LYAMSHEV L. M., 1970, Influence of polymer additives on the pressure fluctuations in a boundary layer, *Sov. Phys. Acoust.*, **16**, 59-63.

KIM J., 1989, On the structure of pressure fluctuations in simulated turbulent channel flow, *J. Fluid Mech.*, **205**, 421-451.

MILLWARD A., LILLEY G. M., 1974, Turbulent pressure fluctuations in water with drag reducing additives, *Proc. Int. Conf. on Drag Reduction*, Paper A1 (Cambridge).

NEKRASSOV B., 1978, Cours d'hydraulique, Ed MIR (Moscou), 95.

PANTON R. L., LINEBARGER J. H., 1974, Wall-pressure spectra calculation for equilibrium boundary layers, *J. Fluid Mech.*, **65**, 261-287.

PANTON R. L., ROBERT G., 1994, The wavenumber-phase velocity representation for the turbulent wall-pressure spectrum. Wall-pressure spectra calculation for equilibrium boundary layers, *J. Fluid Eng.*, **116**, 477-483.

SCHEWE G., 1983, On the structure and resolution of wall-pressure fluctuations associated with turbulent boundary-layer flow, *J. Fluid Mech.*, **134**, 311-328.

SIMPSON R. L., GHODBANE M., MCGRATH B. E., 1987, Surface pressure fluctuations in a separating turbulent boundary layer, *J. Fluid Mech.*, **177**, 167-186.

TOMS B. A., 1948, Some observations on the flow of linear polymer solutions through straight tubes at large Reynolds number, *Proc. 1st Int. Congress on Rheology*, vol. II, North Holland Publ. Co., 135-141.

(Manuscript received May 20, 1996;
accepted October 7, 1997.)